Dynamical Characterization of a Cellulose Acetate Polysaccharide

Miriam Sousa,[†] Ana Rita Brás,[†] Helena Isabel M. Veiga,[‡] Frederico Castelo Ferreira,[§] Maria Norberta de Pinho,[||] Natália T. Correia,[†] and Madalena Dionísio*,[†]

REQUIMTE, Departamento de Química, Faculdade de Ciências e Tecnologia, Universidade Nova de Lisboa, 2829-516 Caparica, Portugal, Instituto de Tecnologia Química e Biológica, Universidade Nova de Lisboa, Av. República, Apart. 127, 2780-901 Oeiras, Portugal, IBB-Institute for Biotechnology and Bioengineering, Centre for Biological and Chemical Engineering, Instituto Superior Técnico, Av. Rovisco Pais, 1049-001 Lisboa, Portugal, and Universidade Técnica de Lisboa, Instituto Superior Técnico, ICEMS/DQEB, 1049-001 Lisboa, Portugal

Received: February 24, 2010; Revised Manuscript Received: June 21, 2010

This work brings together dynamical and structural information at a molecular level for cellulose acetate being an original contribution to the general description of polysaccharide properties. In particular, it allowed reinterpreting the secondary relaxation mechanisms that are still controversial in the literature; a compilation of data provided by different authors is provided. Detailed dynamical information is provided by dielectric relaxation spectroscopy (DRS) ($10^{-1}-10^{6}$ Hz) for cellulose acetate (CA) in the sub-T_g region below ambient temperature; results were compared with cellulose acetate structured as an asymmetric membrane (CAmb). In samples with low water content, two secondary relaxation processes between 173 and 298 K were identified by DRS, associated with localized mobility. The process located at the lowest temperatures (process I) has a different mobility in CA relative to CAmb. The identical crystalline/amorphous state of both materials allowed rationalizing the distinct behavior in terms of polymeric arrangement and ability for water uptake. The looser structure of the CA relative to CAmb as confirmed by FTIR, TGA, and DSC analysis makes more sites accessible to water molecules, resulting in a higher water retention in CA (2.73% w/w) relative to CAmb (1.60% w/w) and an increased molecular mobility in the former due to a plasticizing effect. In both materials, process I is significantly influenced by hydration, shifting to higher frequencies and lower temperatures upon water uptake. This process seems to be associated with mobility occurring within the monomeric unit, which embraces the two anhydroglucose rings connected by the glycosidic linkage and the polar groups directly attached to it. It should involve a very limited length scale, as suggested by its location, far below the glass transition, and the τ_∞ value with a low entropic effect. The relaxation process that emerges later, process II, is similar for both samples being much less influenced by water but experiencing a slight antiplasticizing effect shifting to lower frequencies and higher temperatures upon hydration. It should involve side group motions, strongly coupled to the mobility of the anhydroglucose rings, which become hindered probably due to establishment of H-bonds with water molecules. The plasticizing/antiplasticizing effect is being discussed only on the basis of the frequency position of the relaxation peak. Processes I and II merge into a broad relaxation (γ_{dry}) upon water removal in both CA and CAmb, however evolving slower in the former with drying, due to a more disordered structure of CA that allows water to interact with more internal sites in the polymer. At higher temperatures ($T \geq 353$ K), a process emerges in the high frequency side of the dynamic α-relaxation which is compatible with a β_{JG}-relaxation. The structured specimen CAmb provided an additional way to probe the morphological changes undergone by the material when annealed to temperatures higher than 353 K, originating an increase in the dielectric response. This effect can be associated with a skin densification and partial collapse of the membrane porous network, as observed by SEM.

Introduction

Cellulose is the most abundant natural polysaccharide, and due to its biodegradability and renewability, it has been regarded as the greenest available material (see Scheme 1).[1]

Therefore, a great interest has been devoted to investigating cellulose, including the modification of its structure and properties aiming to expand its potential applications. Among its derivatives, cellulose acetate (CA) has gained special interest in the past few years due to its application, among others, in textiles, food, and pharmaceutical industries.[2] In this context, extensive research has been devoted to the characterization of CA polysaccharides. To gain insight into the molecular mobility that occurs within the polymeric structure, dielectric relaxation spectroscopy (DRS) proved to be a suitable technique to probe its dynamics. DRS studies on different polysaccharides have been reported in the literature, mainly for cellulose[3−6] and for starch.[7,8] Einfeldt et al.[9,10] compiled a large amount of dielectric results of a variety of polysaccharides, including cellulose derivatives, and recognized a common pattern for the detected relaxation processes. Essentially two secondary processes are

* Corresponding author. E-mail: madalena.dionisio@dq.fct.unl.pt.
[†] Faculdade de Ciências e Tecnologia, Universidade Nova de Lisboa.
[‡] Instituto de Tecnologia Química e Biológica, Universidade Nova de Lisboa.
[§] Centre for Biological and Chemical Engineering, Instituto Superior Técnico.
[||] Universidade Técnica de Lisboa, Instituto Superior Técnico.

10.1021/jp101665h
Published on Web 08/06/2010

SCHEME 1: Schematic Representation of Cellulose Structure Evidencing Possible Intra- and Interchain Molecular H-Bonds[a]

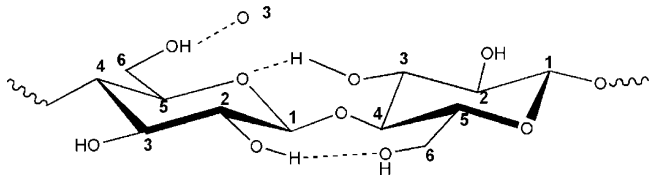

[a] Cellulose is a linear-chain polymer that can be described as being composed of repeating cellobiose disaccharide units which in turn are composed of two anhydroglucose units joined through a $\beta(1,4)$ glycosidic linkage.

observed in the low-temperature range from 138 to 293 K that have been assigned differently by several authors. The diverse interpretations for the origin of these two processes were recently summarized by Kaminsky et al.[11,12] Mainly, the faster relaxation process, designated as γ-relaxation, has been assigned to rotations of side groups[13,14] or motions in the repeating unit having intramolecular character;[12] the second one, observed at higher temperatures, was mainly attributed to local main chain motions involving fluctuations within the glycosidic linkage in nonsubstituted dissacharides.[11] Additionally, this slower relaxation process has also been considered as the precursor of the structural relaxation in polysaccharides[5,15] identified with the Johari−Goldstein relaxation.[12] This process seems to involve the superposition of different contributions, being claimed that it may own some degree of cooperativity.[8,16] However, Diogo and Moura-Ramos[17] in a detailed study by TSDC showed that the components of the distributed secondary relaxation in ethyl cellulose are noncooperative being assigned to local motional relaxation processes; the claimed cooperativity was attributed to the fact that it is an energy distributed process.

In wet cellulosic polysaccharide samples, an additional relaxation process is detected at the room-temperature range. The molecular origin of this process, designated as β_{wet}, is not yet well established; however, it has been assigned to the orientational motions of a mixed phase of both polysaccharide and water (or other swelling solvents), formed in wet systems by a swelling process.[10]

Concerning the importance of water in cellulosic materials, previous studies have shown that water molecules and hydrogen bonds in both inter-and intra-polymer chains play a major role in molecular stabilization and also in the connection between neighboring chains forming microfibrils.[18] These interactions are also responsible for the complexity of the material structure, with the polymer chains forming specific morphologies with systems of holes, pores, and capillaries.[10,15] To investigate the interplay of the hydrogen bond on the polymer matrix and to distinguish different kinds of H-bonds in cellulose acetate, several techniques have been applied, such as FTIR[1,18] and solid state NMR.[19] In particular, Guo and Wu[1] recently investigated the structural evolution of hydrogen bonding in cellulose diacetate upon heating, following the modification of the O−H stretching vibration by FTIR. The interaction of adsorbed water to oxygen atoms was also investigated by NMR[19] where it was observed that water associates preferentially with carbonyl groups in side chains. However, in less structured CA, water molecules access the oxygen atoms easier in both the polymeric side chains and main chain, and thus water can act as a plasticizer. In a different study, Murphy and Pinho[25] provide the detailed assignment of OH modes detected by ATR-FTIR in wet and dry CA asymmetric membrane, establishing a correlation between the water structure and the pore size and the permeation performance.

SCHEME 2: Scheme of Cellulose Acetate Chemical Structure with DS = 2.45

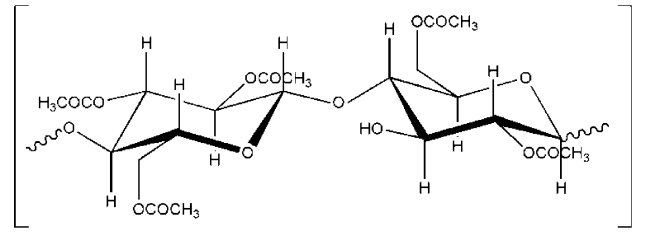

On the other hand, for cellulosic materials submitted to annealing at 453 K, an increase of the dielectric response is reported with a different origin than the rise caused by the presence of water.[20] This effect is attributed to the phenomenon of "hornification" described as irreversible morphological changes (see ref 20 and references therein).

Despite the numerous experimental studies devoted to the secondary mobility of cellulose and its derivatives, both in wet and dried states, the molecular motions underlying the different relaxation processes are still a matter of debate.[11,12,17]

Therefore, the present dynamical study by DRS focused on the subglass mobility in cellulose acetate (CA) intends to be an additional contribution to the comprehension of the molecular origin of the detected relaxation processes. Furthermore, cellulose acetate will be investigated in this work under two structurally/morphologically different forms: the initial polymeric state and structured as a membrane. The latter offers a way to further evaluate by a microscopy technique such as SEM the effect of annealing the material at high temperatures.

To complement the dynamical description, a physicochemical characterization was also carried out by FTIR, SEM, DSC, and TGA, allowing correlating structural properties of the CA polysaccharide and its dynamical behavior. This approach for a porous membrane is a pioneer in the literature, to our best knowledge.

Experimental Section

Materials. Cellulose acetate (see Scheme 2) was purchased from Eastmann Kodak. It had a molecular weight (MW) of 30 270 and an acetyl content of 39.8% corresponding to a substitution degree, DS, i.e., the average number of acetyl groups in each glycosidic repeat unity, of 2.45 (a completely substituted material will have a DS of 3).[21]

Membrane Preparation. Two different sets of samples were tested: (i) cellulose acetate (CA) as received and (ii) asymmetric cellulose acetate membrane (CAmb). Due to the practical importance of asymmetric membranes in ultrafiltration, nanofiltration, and reverse osmosis,[22−25] the respective membrane manufacture conditions are well reported in the literature,[22,26−29] allowing one to produce membranes with asymmetric structures, consisting of a dense skin layer (0.1−1 μm) on top of a highly porous and thick structure (100−200 μm).

The membrane used in this work was prepared by the phase inversion method under identical conditions to those reported in refs 25 and 29 and using a casting solution of 17% w/w CA powder and formamide (less solvent): acetone (solvent) in a concentration ratio of 32:51% w/w.

The membrane was then gently dried as described by Lui et al.:[30] by immersing in aqueous isopropanol solutions of successively higher alcohol contents following immersion in isopropanol/hexane solutions of successively higher hexane

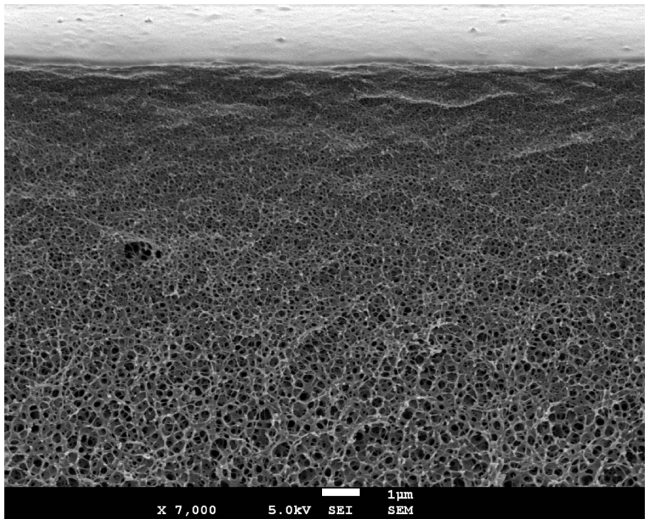

Figure 1. SEM image of the asymmetric CA membrane (7000×) evidencing the asymmetric structure with a dense layer in the top part and a more open porous network in the bottom.

contents in order to remove the more polar solvent and slowly accommodate the membrane structure to a less polar environment. The hexane was then removed by gentle evaporation in a desiccator at room temperature (295−298 K) for 13 days. The obtained average membrane thickness was about 80 μm.

Conventional drying processes like thermo-vacuum treatment were not undertaken, since a complete drying of the membrane can irreversibly damage and/or destroy the membrane structure.[31]

Notice that membrane preparation does not involve any chemical or physical modification of the polymer structure and the different architectures obtained for the membrane samples are only obtained by dissolution of the polymer on solvents and controlling solvent evaporation and polymer precipitation rates.

Sample Characterization. ***Scanning Electron Microscopy.*** The membrane morphology at a microscale was characterized through scanning electron microscopy (SEM) imaging using a Hitachi S2400, fitted with a Rontec standard energy dispersive (EDS) detector. In order to get the membrane cross section, the sample was freeze-fractured in liquid nitrogen. The sample, with about 0.5 cm^2 area, was mounted onto the aluminum stubs using carbon cement (D-400, Neubaeur Chemikalien), and a thick coating of 3 ± 6 nm gold particles was deposited using a dual ion beam sputter coater.

Figure 1 presents the respective SEM micrograph, providing an overview of the membrane cross section. From the snapshot, it is possible to visualize the asymmetric structure of the membrane: the dense skin layer is located in the upper side where the resolution of the microscope does not allow distinguishing nanopores; the increasing dimension of the pores in the network becomes evident from top to bottom.

Thermal Analysis. *Thermogravimetry* experiments (TGA) were performed in a TA Instruments model TGA Q50, using high purity nitrogen (water free) as a purge gas at a flow rate of 60 mL·min^{-1}. TGA data were obtained in open aluminum pans. The samples, with an initial weight of ∼10 mg (cellulose acetate powder) and ∼3 mg (membrane), were submitted to the following temperature scan: (i) a temperature ramp from 298 up to 383 K, (ii) an isotherm at 383 K for 10 min, and (iii) a second ramp up to 973 K. In paths i and iii, the heating rate was set to 10 K·min^{-1}.

Thermogravimetry was performed to quantify the water content and monitor decomposition in both samples. Although

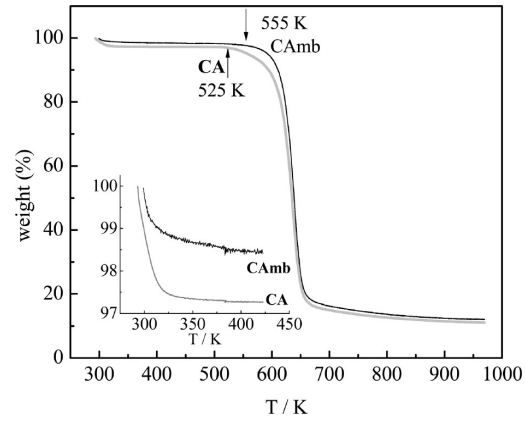

Figure 2. Thermogravimetric curves obtained on heating at 10 K·min^{-1} for the as received cellulose acetate (CA) and membrane (CAmb). Inset: Detailed view evidencing the temperature region (up to ∼423 K) where the mass loss is due to water release. The onset of thermal decomposition of each sample is indicated by the arrows.

the asymmetric CA membrane was subjected to a solvent drying procedure, it is known that, due to its hydrophilicity, CA materials promptly recapture water by the hydroxyl and acetyl groups through hydrogen bonds.[1]

Figure 2 shows the thermograms obtained for both CA and CAmb. The water content in each sample, corresponding to molecules which are weakly bonded, physically adsorbed in the surface, and inside the pores, was estimated from the weight loss observed from the beginning of the temperature scan until around 423 K (see a scale-up in the inset): the estimated values were 2.73 and 1.60% w/w for CA and CAmb, respectively. The major mass loss detected by TGA is due to decomposition of the CA matrix having a starting temperature around 525 and 555 K, respectively, for CA and CAmb, and occurs up to 700 K.

Differential Scanning Calorimetry. DSC measurements were performed in a SETARAM DSC 131 calorimeter. Dry high purity N_2 gas was purged through the sample during the measurements. Both CA and CAmb were analyzed. The samples were heated up to 543 K (membrane sample mass ∼5 mg) and 573 K (CA mass ∼18 mg). The thermograms were collected at 10 K·min^{-1}.

Infrared Spectroscopy. Infrared spectra of both (i) KBr pellet of cellulose acetate powder with 3% (weight of CA/KBr) and (i) CAmb were recorded, at room temperature, using an ATI Mattson Genesis Series Fourier transform infrared spectrometer. Spectra were taken with a resolution of 4 cm^{-1}; 64 scans were averaged.

Dielectric Relaxation Spectroscopy. For the analysis of the cellulose acetate as received (CA), approximately 40 mg of this powder was compressed under a pressing force of ∼50 kN, to produce a disk (∼10 mm diameter). The membrane was cut into disks of about 20 mm in diameter for the dielectric spectroscopy measurements. The samples were then placed between two gold plated electrodes in a parallel plate capacitor, BDS 1200. The sample cell was mounted on a cryostat, BDS 1100, and exposed to a heated gas stream being evaporated from liquid nitrogen in a Dewar. The temperature control was assured by the Quatro Cryosystem and performed within ±0.5 K (all modules supplied by Novocontrol). The complex dielectric function $\varepsilon^*(f) = \varepsilon'(f) - i\varepsilon''(f)$ (f, frequency; ε', real part; ε'', imaginary part) was measured by an Alpha-N analyzer also from Novocontrol GmbH, covering a frequency range from 10^{-1} Hz to 1 MHz. After an initial cooling ramp at 10 K·min^{-1}, from

SCHEME 3: Profile of the Temperature Procedure in the Thermal Cycling DRS Experiments

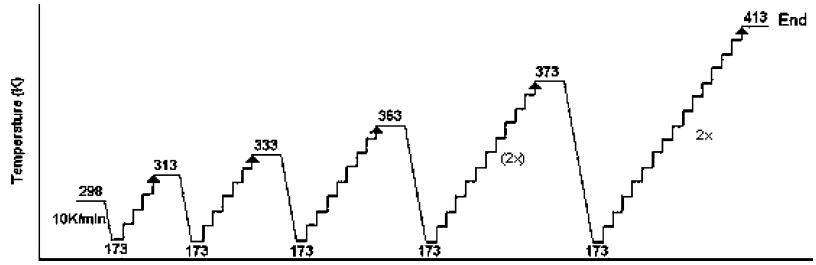

298 to 173 K, isothermal dielectric measurements were carried from 173 to 298 K, in steps of 5 K.

To analyze the influence of dehydration, an additional experiment was performed. Each sample was submitted to thermal cycling by measuring isothermally in successive runs starting always from $T_i = 173$ K, in steps of 5 K, up to successive higher final temperatures (T_f); each time that the frequency scan is completed at the final presetted T_f, the sample is cooled down to 173 K and a new run begins up to a higher end temperature ($T_f = 298$, 313, 333, 353, 373 (2×), and 413 K; see Scheme 3).

For dried CA, isothermal measurements were extended up to 473 K.

The dielectric relaxation data obtained were deconvoluted using a sum of the model function introduced by Havriliak−Negami:[32]

$$\varepsilon^*(\omega) = \varepsilon_\infty + \sum_j \frac{\Delta\varepsilon_j}{[1 + (i\omega\tau_j)^{\alpha_{HNj}}]^{\beta_{HNj}}} \qquad (1)$$

where j is the number of relaxation processes, $\Delta\varepsilon = \varepsilon_s - \varepsilon_\infty$ is the dielectric strength, i.e., the difference between the real permittivity values at, respectively, the low and high frequency limits, $\tau \approx (2\pi f_{max})^{-1}$ is the characteristic relaxation time, and α_{HN} and β_{HN} are the shape parameters ($0 < \alpha_{HN} < 1$, $0 < \alpha_{HN} \cdot \beta_{HN} < 1$). When the data are influenced by low frequency conductivity contribution, an additional term $i\sigma/\omega^c\varepsilon_0$ was added to the dielectric loss, where ε_0 is the vacuum permittivity, σ and c are fitting parameters: σ is related to the dc conductivity of the sample and the parameter c ($0 < c \leq 1$) describes for $c = 1$ Ohmic and for $c < 1$ non-Ohmic effects in the conductivity. From the estimated values of τ_{HN}, α_{HN}, and β_{HN} fitting parameters, it is possible to estimate a model-independent relaxation time, τ_{max} ($= 1/2\pi f_{max}$) (for details, see refs 33 and 34).

Results and Discussion

Differential Scanning Calorimetry (DSC). The thermal properties of the tested samples were investigated by DSC in addition to TGA (see the Experimental Section). The respective thermograms are presented in Figure 3.

In a first stage, an endotherm is detected from room temperature to around 380 K due to water removal (Figure 3a). The endotherm for CA is broader and more intense than that for CAmb, being compatible with higher water content as determined by TGA. The higher broadness can also be an indication of a wider distribution of different accessible sites for water uptake in the powder. At higher temperatures (Figure 3b), above 460 K, the main event is an endothermic peak due to melting; both samples undergo decomposition (data not shown) for higher temperatures.

The thermograms do not show clear evidence of the glass transition. Reported values in the literature for the glass transition temperature (T_g) for CA with the same acetyl content (39.8%) scatter a little, depending on the determination method. Nevertheless, an independent behavior relative to the molecular weight was found, as determined by DSC[35] with a T_g value of 472.5 K in good agreement with those obtained from DMTA[36] and DSC,[16] 470 and 463 K, respectively. Taking into account these values and the occurrence of some overlapping between the glass transition and the melting endotherm,[35] a close inspection of the CA thermogram shows that a discontinuity in the heat flux precedes melting that has the appearance of a glass transition. The onset of this thermal event occurs at 467 K, fitting well with the reported T_g values. At approximately the same location, a similar feature is observed for the thermogram of the membrane; the dashed square in Figure 3b delimits the region where the glass transition signature is detected. Therefore, the simultaneous detection of a glass transition and a melting endotherm means that all of the analyzed specimens are in a semicrystalline state.

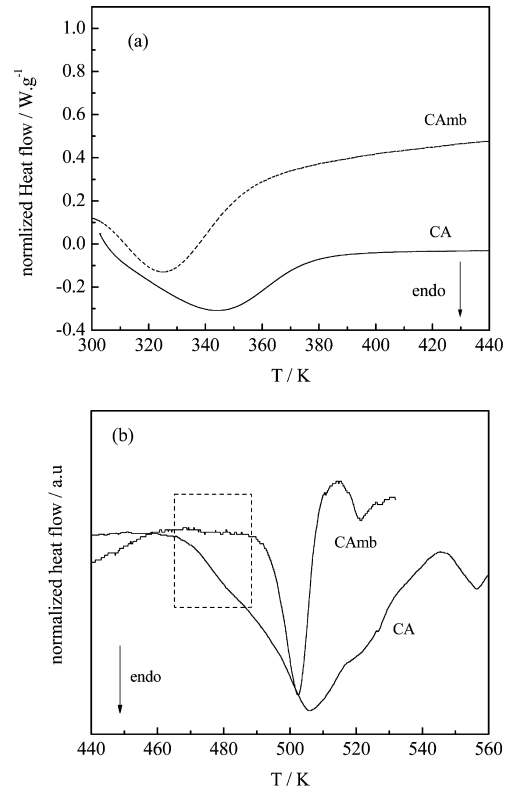

Figure 3. DSC thermograms for cellulose acetate (CA) and membrane (CAmb), obtained on the first heating run at 10 K·min^{-1}: (a) endothermic peak due to water loss; (b) glass transition region (inside the dashed area) and endothermic peak due to melting (above 480 K).

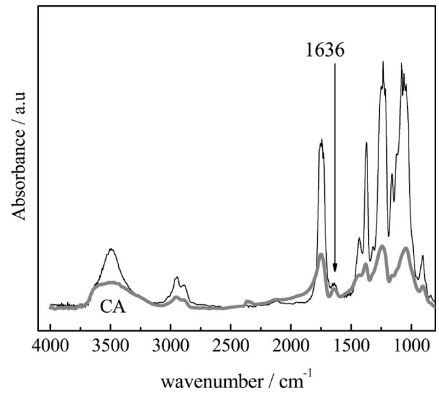

Figure 4. FTIR spectra of CA (gray line) and CAmb (black line), with indication of the adsorbed water peak centered at 1636 cm^{-1}.

It is interesting to note that the melting endotherm is much sharper for the membrane having a peak location at 502 K. This value fits within the reported temperature range (500−520 K) for the melting of CA with DS = 2.46.[16,35] The broadness of the melting endotherm in CA could indicate a less perfect crystalline arrangement relative to the membrane. This conclusion seems to be corroborated by previous TGA analysis. In fact, it was previously observed for celullose acetate that a better chain packing leads to higher thermal stability;[37] therefore, the inferior onset for degradation of CA indicates a less ordered chain arrangement than that for the membrane sample.

The crystallinity degree was estimated by the ratio between the melting enthalpy of the material under study (ΔH_m) and the respective value for the totally crystalline material, (ΔH_m°), i.e.,

$$\chi_c(\%) = \frac{\Delta H_m}{\Delta H_m^\circ} \times 100 \qquad (2)$$

where $\Delta H_m^\circ = 58.8\ J \cdot g^{-1}$ as proposed by Cerqueira et al.[38] The melting enthalpy value calculated from the thermogram for CAmb was 6.8 $J \cdot g^{-1}$. For CA, it is difficult to accurately determine ΔH_m due to the high overlap between the melting endotherm and the glass transition. However, a value of 6.8 $J \cdot g^{-1}$ was also obtained. From eq 2, it was possible to estimate the crystallinity degree, χ_c, as 12% for both CA and CAmb. In spite of the uncertainty affecting the value of χ_c for CA, the two samples have very similar low crystallinity degrees, being mainly amorphous.

Infrared Spectroscopy. In Figure 4, the FTIR spectra for CA and CAmb are presented. The small water content determined by TGA is confirmed. Indeed, the low intensity of the band located between 3200 and 3600 cm^{-1}, corresponding to the overlapping of different vibration bands in the OH stretching region, and of the peak at 1636 cm^{-1} (bending of adsorbed water),[25] corroborates the presence of low water amounts. Note that the peak at 1636 cm^{-1} is used to directly observe the state of water in CA membrane, since it does not overlap with any bands of cellulose acetate materials, which occur below 1600 cm^{-1},[39] being almost absent in dried samples. Another observation is the lower resolution of the CA spectrum as compared with membrane which can be taken as an indication that CA powder is less structured.

To investigate the hydrogen bonds via inter- and intrachain and adsorbed water, the region of OH stretching modes (3800−3100 cm^{-1}) will be further analyzed in more detail.

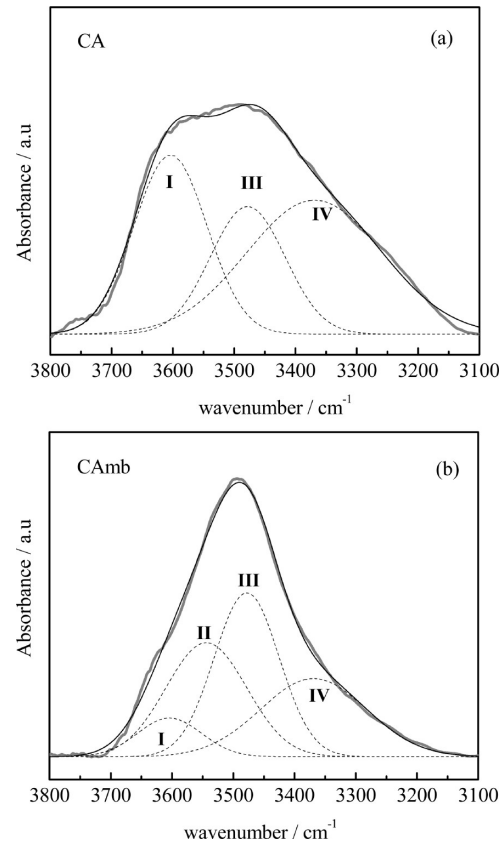

Figure 5. Deconvolution with Gaussian peaks of the OH stretching region, 3800−3100 cm^{-1}, for (a) CA and (b) CAmb. Components I−IV centered, respectively, at 3604 cm^{-1} (absorbed water), 3544 cm^{-1} (free O−H stretching), 3478 cm^{-1} (intrachain H-bond ν_1 for dehydrated CA), and 3369 cm^{-1} (intrachain H-bond ν_2).[1]

Figure 5 presents the deconvolution of this band for (a) CA and (b) CAmb.

A set of Gaussian bands was fitted to the spectrum, where the maximum position of each single component corresponds to the wavenumber provided recently by Guo and Wu:[1] 3604 cm^{-1}, peak I (absorbed water); 3544 cm^{-1}, peak II (free O−H stretching); 3478 cm^{-1}, peak III (intrachain H-bond ν_1 for dehydrated CA); 3369 cm^{-1}, peak IV (intrachain H-bond ν_2). In a first attempt, a fifth component at 3409 cm^{-1} assigned to interchain H-bond was also considered;[1] however, the contribution of this Gaussian band to the fitting of the obtained sample spectra was always negligible, and thus not considered. The sum of the relative weight contributions of the intramolecular components (bands III and IV) is identical in both CA and CAmb.

As a main observation, the high relative weight of component I and the absence of component II in CA should be mentioned. Peak I is assigned to absorbed water, and thus, this result confirms the previous relative TGA water quantification. Furthermore, the negligible value of peak II, associated with free O−H stretching, seems to corroborate the higher levels of hydration of CA relative to CAmb, with the majority of OH groups in the polymer unavailable for interchain interactions, since they are hydrogen bonded to water molecules. Notice that only a few OH free groups exist in the monomeric unit. The acetylation degree of 39.8%, which is intermediate in chemical composition between cellulose diacetate and triacetate, corresponds to 0.55 of unacetylated hydroxyl groups per anhydroglucose unit,[40] i.e., one OH group per monomer. In a raw estimate, the molar mass of two anhydroglucose units linked

TABLE 1: Summary of the Different Parameters for Cellulose Acetate Powder (CA) and Structured as Membrane (CAmb), Determined from TGA (Water Content), FTIR (Crystallinity Index), and DSC (Melting Enthalpy and Crystalline Degree)

sample	water content (% w/w) (TGA)	crystallinity index (FTIR)	crystallinity degree (%) (DSC)	ΔH_m ($J \cdot g^{-1}$) (DSC)
CA	2.73	1.4	12	6.8
CAmb	1.60	1.3	~12	~6.8

by an oxygen atom containing only one free OH is around 500 $g \cdot mol^{-1}$; thus, a percentage of 2.73% w/w, as found for the water content in CA, is 14 $g \cdot mol^{-1}$, which roughly corresponds to one water molecule per monomeric unit. In the limit, assuming that each water molecule is H-bonded to a single OH group, no free OH groups will be left in the CA powder. Moreover, given that the nonsubstituted OH groups are responsible for the establishment of interchain interactions,[41] it is not surprising that no component in the FTIR spectra associated with these intermolecular OH− vibrations was found. Furthermore, since the acetyl side groups are unable to establish H-bonds between neighboring chains, it may be concluded that the studied CA samples do not form microfibrils.[18] As the interchain interactions are responsible for the three-dimensional order that is in the origin of the crystalline fraction, their absence thus corroborates the highly amorphous nature of the studied CA samples as found by DSC.

To get further insight into the crystallinity of the samples, the crystallinity index, which is a measure of how far an unknown sample is between the extremes of the most amorphous and most crystalline samples obtainable for a polymer species,[42] was estimated from FTIR data. The ratio of the absorbance at 1425 and 900 cm^{-1} is often used to evaluate the crystallinity index in cellulosic materials.[43−45] The values thus estimated for both samples were similar, indicating that no major differences exist between the crystallinity ratios of the tested specimens.

This is coherent with the similarity in the crystallinity degrees estimated from DSC; therefore, CA and CAmb have an identical amount of crystalline phase.

A summary of the properties determined by thermal and infrared analysis is presented in Table 1.

Dynamic Molecular Characterization. ***Dielectric Measurements Taken from Runs up to 298 K.*** Dielectric relaxation spectroscopy (DRS) probes the molecular dynamics through the motions of dipoles, which fluctuate under the influence of an outer oscillating electric field. The measured dielectric permittivity, $\varepsilon^*(\omega) = \varepsilon'(\omega) - i\varepsilon''(\omega)$, is a complex quantity whose real part ($\varepsilon'(\omega)$) decreases as a sigmoid curve and the imaginary part ($\varepsilon''(\omega)$), also designated as dielectric loss, passes through a maximum at f_{max} ($\tau_{max} = 1/2\pi f_{max}$), when the dipoles are no longer able to follow the electric field oscillations. The maximum location allows inferring about molecular mobility.

The dielectric loss spectra, $\varepsilon''(\omega)$, of the CA samples were collected up to 298 K. Taking into account the glass transition temperature estimated from the onset in DSC scan (around 467 K), this study of the dielectric behavior corresponds to subglass mobility that should occur in the disordered amorphous regions. The spectra for CA (2.73% w/w water content) are presented in Figure 6 covering the temperature range from 178 to 268 K (shown in steps of 10 K). As expected, the maximum of each spectrum is shifted to higher frequencies as the temperature increases due to an enhancement of dipolar mobility.

Figure 7a compares the $\varepsilon''(\omega)$ isotherms at 198 K of CA (full symbols) with CAmb 1.60% w/w water content (open symbols).

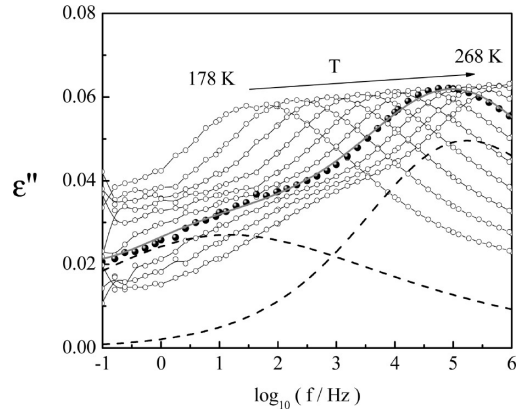

Figure 6. Frequency dependence of the imaginary part of the complex dielectric permittivity from 178 to 268 K in steps of 10 K, for CA (2.73% w/w water content). Isothermal data collected at 238 K (full symbols) is highlighted to illustrate the HN fit: dashed lines are the individual HN functions, and the solid line is the overall HN fit.

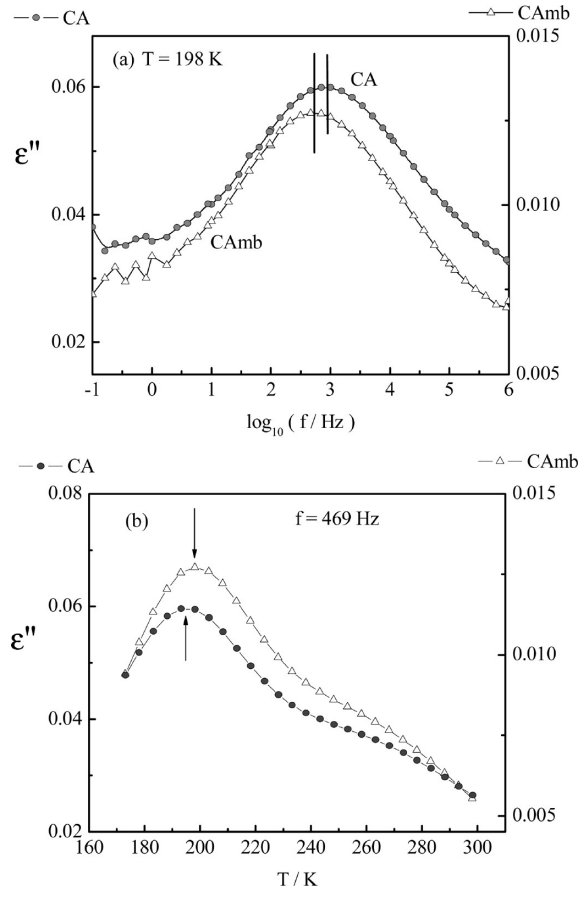

Figure 7. Comparison between the dielectric behavior of CA (full symbols) and CAmb (open symbols): (a) dielectric loss collected at 198 K; (b) isochronal plots. The bars evidence the displacement between the maxima of the dielectric response obtained for each sample under comparison.

First, the higher dielectric strength of the CA spectrum is justified by the greater water uptake in this sample, since the high dipole moment of water molecules is associated with the polymer relaxational behavior (the plot of CAmb is presented in the secondary *y* axis in the right side; the lower dielectric response is confirmed by the normalized tan δ plots ($= \varepsilon''/\varepsilon'$), which are independent of sample thickness). Second, the maxima location is different, the relaxational behavior of the membrane being slightly slower than CA, as denoted by

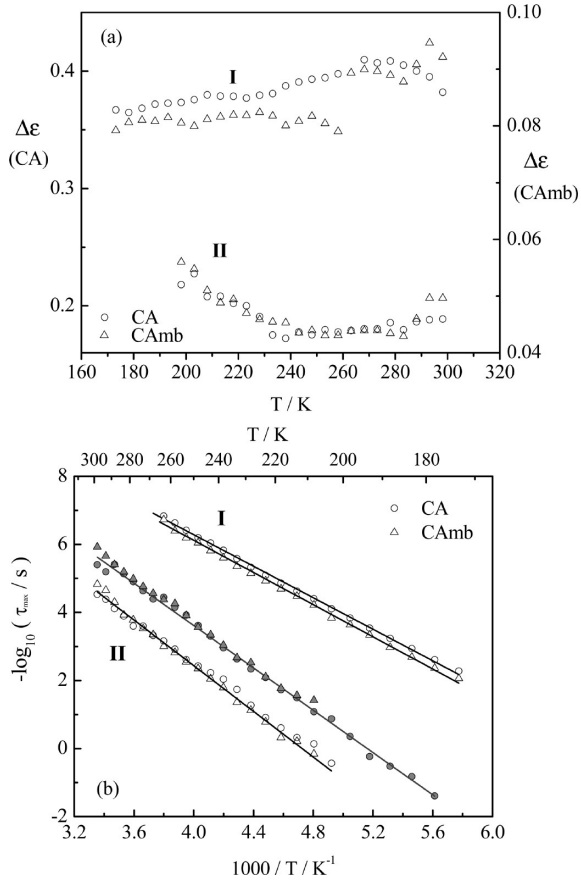

Figure 8. Temperature dependence of (a) dielectric strength, $\Delta\varepsilon$, and (b) relaxation times, τ_{max}, for processes I and II detected in CA (2.73% w/w water) and CAmb (1.60% w/w water)—open symbols. Full symbols stand for $\tau_{max}(T)$ of the remaining process in both samples after dehydration.

the shift to lower frequencies of the dielectric loss peak of CAmb. The same effect can be visualized in a different representation where loss data are plotted at a fixed frequency against temperature (isochronal plot). This is shown in Figure 7b at 469 Hz, where the maximum position of the CA main peak slightly deviates to lower temperatures, evidencing its enhanced mobility relative to the process detected in the membrane.

A close inspection of the obtained spectra reveals that two subglass relaxation processes are detected for both CA and CAmb; the isochronal plot enhances this bimodal character. To obtain a better description of the underlying processes, a sum of two Havriliak−Negami (HN) functions[32] was fitted to the $\varepsilon''(\omega)$ raw data (see the Experimental Section). The individual HN functions at 238 K are shown as dashed lines in Figure 6, while the overall fit is presented as a solid gray line, evidencing how the fitting procedure adequately describes the raw data. To help further discussion of the detected process, it will be designated as processes I and II in decreasing order of frequency (increasing order of temperature). The HN fit shape parameters, α_{HN} and β_{HN}, are 0.36 ± 0.01 and 0.77 ± 0.02 for process I and 0.39 ± 0.03 and 0.53 ± 0.05 for process II, respectively, for both CA and CAmb. The estimated dielectric strength and the respective temperature dependence for both processes are plotted in Figure 8a. Almost opposite dependences were found: the magnitude of the faster process (I) generally increases with the temperature, while, in the slower process (II), $\Delta\varepsilon$ slightly decreases as the temperature increases. The respective sum is nearly constant. This behavior is in close agreement with what was found by Kaminsky et al.[11] for the temperature dependences of the dielectric strengths of the two secondary processes found in different sugars.

The relaxation times also estimated from the HN fits, after conversion to τ_{max} (see Experimental Section), are plotted against the reciprocal of temperature in Figure 8b (open symbols). As a main feature, both processes evolve linearly with the temperature; i.e., an Arrhenius-type temperature dependence is obeyed. Furthermore, the activation plot highlights the observations previously discussed: (i) for process I, the relaxation rate of CA is faster than CAmb (remember Figure 7a); (ii) the position of process II is almost invariant while comparing both CA and membrane.

From the slope of the linear temperature dependence of the relaxation times, it is possible to estimate an activation energy, according to the Arrhenius relationship: $\tau(T) = \tau_\infty \exp(E_a/k_B T)$ (where E_a is the activation energy representing the energy barrier for molecular rearrangement, τ_∞ is the time at infinite temperature, k_B is Boltzman's constant, and T is the absolute temperature). For process I, $E_{a,I} = 44.3 \pm 0.4$ and 45.3 ± 0.6 kJ·mol^{-1}, respectively, for CA and CAmb, and for process II, $E_{a,II} = 64.3 \pm 0.8$ kJ·mol^{-1} for both systems. The pre-exponential factor has the same value for both processes, $\tau_\infty = (3 \pm 1) \times 10^{-16}$ s.

As mentioned previously in the Introduction, there is a lack of consensus in the literature concerning the molecular origin of the secondary relaxations in carbohydrates. In a recent publication by Kaminsky et al.,[12] a summary of the different attributions to similar processes is made. The faster relaxation (designated γ by the majority of authors), with activation energies between 32 and 52 kJ·mol^{-1}, is attributed by Nishinari et al.,[14] Montès et al.,[13] Starkweather et al.,[46] and the authors themselves to mainly localized motions with negligible entropy; the local motion character, intramolecular in nature, was confirmed by its insensitivity to pressure.[12,47]

Both pre-exponential factor (τ_∞) and activation energy (E_a) values estimated here for process I are very close to the ones previously reported for the γ-process found in different sugars which do not possess any acetyl side group, e.g., the disaccharides maltose and lactose which have, respectively, ($\tau_\infty \sim 5 \times 10^{-16}$, $E_a = 47$ kJ·mol^{-1}) and ($\tau_\infty \sim 9 \times 10^{-16}$, $E_a = 44$ kJ·mol^{-1}).[11] Therefore, it is possible to conceive a molecular motion other than independent rotations of lateral groups. In fact, the assignment of this process to exocyclic group rotations was ruled out previously by NMR studies[48] for the monosaccharide glucose where it was observed that rotational freedom for the methylol side group does not result in additional motion, since a strong correlation was found between the mobility of the CH_2OH group and the glucose ring.

In a very recent work, Kaminsky et al.[49] reinforce this observation, finding no significant differences in the γ-process between lactose and octa-*O*-acetyl-lactose: the former only carries hydroxyl groups while in the latter all of the hydrogen atoms from OH groups were replaced by acetyl moieties, revealing a common origin for the underlying mechanism in both materials.

Einfeldt et al.[8] designate the lower temperature process as β (instead of γ as the designation adopted by the majority of the authors, since this process is located at higher frequencies), attributing it to local main chain motions involving the (1−4)β glycosidic linkage. This process in commercial cellulose acetate (DS = 2.45) has an activation energy of 46.8 kJ·mol^{-1} in close agreement to process I here reported.

In CA, the authors detect a second process at lower frequencies with an activation energy of 50.1 kJ·mol^{-1}, attributed to

reorientations of the acetyl side groups in the positions C2 and C3 (γ-(C_2−O−Ac and C_3−O−Ac) in short $\gamma(C_2,C_3)$). The existence of additional processes relative to cellulose was observed for cellulose-like oligomers such as cellobiose or β-cyclodextrin and derivatives of cellulose and starches.[9,10,50] They are called γ-C-side group processes and are associated with the reorientation of more or less bulky side groups, implying a simultaneous motion of the main chain for spatial reasons.[50] Consequently, the position and the distribution on the frequency scale of these γ-C-side group relaxations are indirectly determined by the dominant β-relaxation (process I in the present work or the usually designated γ-relaxation). In some substituted cellulose materials, e.g., hydroxyl-propyl-cellulose, the γ-C-side group process is more intense, becoming more resolved from the low temperature process.[9,10,50] Moreover, a dependence on the degree of substitution was observed in such a way that all relaxations can be separated in the dielectric spectra only for derivatives with low DS; the position of the substituent group at the anhydroglucose unit also influences the side group relaxation.[50]

This kind of side-group-related process is distinct from the β-relaxation detected in cellulosic materials without substituent groups, which is claimed by several authors as involving restricted motions of the main chain segments[12,13,51] and being the precursor of the structural relaxation.[5] It is also identified with the Johari−Goldstein (JG) relaxation for well dried disaccharides.[12] This process always becomes faster and its intensity increases upon hydration; it is sensitive to physical aging and senses the pressure like the α-relaxation associated with the dynamic glass transition as summarized in Table 2, where a compilation of literature data is provided.

To discern if process II detected in this work for CA is a β_{JG}-process instead of the slower process due to the influence of bulky side groups, an unequivocal definition of the shape of the α-process would be required, allowing a proper estimation of the β_{KWW} parameter; the latter parameter determines the location of β_{JG} according the coupling-model theory as proposed by K. Ngai.[52] Due to the influence of conductivity that masks the reorientational dielectric response, it was not possible to define the α-process associated with the dynamic glass transition and, thus, to estimate τ_{JG}. The temperature dependence of the dielectric strength observed in this work for process II (Figure 8a) nicely compares with the behavior found for the β_{JG}-relaxation observed for several sugars including, e.g., lactose,[11] which could lead us to conceive a similar origin for process II detected in CA. Nevertheless, the temperature range where the β_{JG}-process of lactose is observed is much higher than that at which process II is detected for CA, the latter having a superior T_g value ($T_{g,CA} \sim T_{g,lactose} + 80$ K). Thus, it will be expected that the process precursor of the α-relaxation will appear at a higher temperature for CA. Moreover, the pre-exponential factor, τ_∞, found for the β-process detected by DRS in polysaccharides is, in general, lower than the one obtained for CA either as membrane or powder ($\tau_\infty = 3 \times 10^{-16}$ s) lying within the range $10^{-17}-10^{-20}$ s.[13,51] Values of the pre-exponential factor, τ_∞, lower than the value predicted for a Debye-type process ($\sim 10^{-12}-10^{-14}$ s) correspond to an activation entropy greater than zero, according to the Eyring formalism,[53] being associated with molecular mechanisms involving some degree of cooperativity. In process II, the entropic effect is not so accentuated. Therefore, it seems unlikely that process II in CA is associated with a β_{JG}-relaxation; this will be further clarified in the next section.

Dielectric Measurements Taken from Runs up to 413 K: Influence of Dehydration. To get further insight into the origin of these processes, several studies have been performed in hydrated and dried samples. As mentioned in the Introduction, distinct results are reported concerning the water effect over the secondary relaxations in polysaccharides. For instance, Montès et al.[13] through dynamic mechanical analysis (DMA) of cellulose and Laredo et al.[51] using the thermally stimulated depolarization currents (TSDC) technique to analyze starch both found that water plasticizes the β-process by decreasing its respective activation energy and insignificantly influences the γ-process. In starch,[51] two secondary processes are observed at the lowest temperatures, γ_1 and γ_2, both insensitive to water (E_a, $\tau_{\infty(TSDC)}$ = (40 ± 2 kJ·mol^{-1}, $10^{-14.3\pm0.2}$ s)$_{<15,5\%wet}$ and (42 ± 2 kJ·mol^{-1}, $10^{-13.8\pm0.1}$ s)$_{dry}$ for γ_1; (28 ± 2 kJ·mol^{-1}, $10^{-11.6\pm0.5}$ s)$_{<15,5\%wet}$ and (25 ± 2 kJ·mol^{-1}, $10^{-10.6\pm0.5}$ s)$_{dry}$ for γ_2); the average value of these activation energies is in close agreement with the E_a value estimated for the γ-relaxation observed in amorphous cellulose[13] (E_a, $\tau_{\infty(DMA)}$ = (34 kJ·mol^{-1}, 10^{-13} s)$_{\le 6\%wet}$ and (36 kJ·mol^{-1}, 10^{-12} s)$_{dry}$). On the other hand, Jafarpour and co-workers[5,6] report how water affects differently the two secondary relaxations in microcrystalline cellulose, studied by TSDC ($f \sim 10^{-3}$ Hz): (i) a plasticizing effect was observed for the β-process that deviates to lower temperatures and decreases the respective activation energy, and (ii) an antiplasticizing effect was observed over the γ-relaxation where an increase of the activation energy and a shift to higher temperatures was found with water uptake; for the same γ-process, the authors observed by DRS[5] a decrease in the activation energy and an increase of the pre-exponential factor upon dehydration (E_a, $\tau_{\infty(DRS)}$ = (50.9 ± 0.2 kJ·mol^{-1}, (1.2 ± 0.1) × 10^{-17} s)$_{4\%wet}$ and (35 kJ·mol^{-1}, 10^{-13}s)$_{dry}$); however, the peak position of the relaxation process shifts to lower frequencies for spectra collected at $T \ge 183$ K.[54] A similar behavior is reported by Einfeldt et al.[10,20] for the relaxation observed at the lowest temperatures (called β by the authors) in different types of cellulose (both amorphous and semicrystalline) studied by DRS: a decrease of the activation energy (E_a, $\tau_{\infty(DRS)}$ = (55.0 kJ·mol^{-1}, 1 × 10^{-18} s)$_{10\%wet}$ and (42.5 kJ·mol^{-1}, 3 × 10^{-15} s)$_{dry}$), and a shift of the position of the relaxation peak to lower frequencies is also found. Table 2 summarizes the activation parameters provided for the monosaccharide glucose[55−57] and several polysaccharides in both dried and wet state. Besides hydration, the influence of physical aging and pressure, when reported in the literature, in the secondary relaxations is also described.

The estimated activation parameters for the γ-relaxation as investigated by TSDC and DMA, either in the wet or dried state, are compatible with very localized mobility with pre-exponential factors close to the Debye prefactor. By DRS, in general, lower pre-exponential factors are found, since for an energy distributed process the technique probes a mean relaxation time.

In the present work, to evaluate the influence of dehydration in the secondary processes observed in cellulose acetate, dielectric measurements were isothermally performed in both CA and CAmb in successive runs starting from 173 K up to increasing final temperatures (thermal cycling as described in Experimental Section), with each successive run corresponding to drier samples. Figure 9 shows the isochronal plots of tan δ ($= \varepsilon''/\varepsilon'$) for the different runs for (a) CA and (b) CAmb; the last run is illustrated in full circles corresponding to data collected after attaining 413 K.

Interesting enough, it is the dramatic influence of water in the dielectric spectrum, even at such small amounts as the one

TABLE 2: Summary of the Activation Energy, E_a, and the Pre-Exponential Factor, τ_∞, of the Arrhenius Fit, $\tau(T) = \tau_\infty \exp(E_a/k_BT)$, Obtained by DRS, TSDC,and DMA for Secondary Relaxations Observed in the Glassy State of Glucose and Several Polysaccharides, in the Dried and Wet States[a]

Saccharide (mono and poly)	Faster process (designated as γ) (lower T)			Slower process (designated as β) (higher T)			water % w/w	Reference
	Dry E_a, τ_∞ (kJ/mol, s)	Wet E_a, τ_∞ (kJ/mol, s)	Comments	Dry E_a, τ_∞ (kJ/mol, s)	Wet E_a, τ_∞ (kJ/mol, s)	Comments		
D-glucose	42, 3.1×10^{-14} [b]	59, 7.9×10^{-17} [b]	Shift to higher T	---	---	---	10	Noel *et al.*[55] (DRS)
	42, 1×10^{-15}	-------	~Insensitive to pressure	76, 1.3×10^{-16}	----	Shift to lower *f* with increasing pressure	---	Kaminski *et al.*[49,56] (Brodband DRS)
	Non-cooperative process; Insensitive to physical aging			Non-cooperative process; Very sensitive to physical aging			---	Diogo and Moura Ramos[57] (TSDC, f~10^{-3} Hz)
Cellulose	Called β -relaxation by the authors		~insensitive for water up to 4%; Shift to higher *f* and *Intensity increases*	Hydrated samples: a slower relaxation is identified as β -wet process; Extremely dried samples a very broad and weak process is observed (called δ-relaxation by the authors) in the same frequency range			10	Einfeldt *et al.*[10,20,50] (DRS)
	42.5, 3×10^{-15}	55.0, 1×10^{-18}						
	35, 1×10^{-13}	50.9, 1×10^{-17}	Shift to higher *f* (T≥183 K) [c]	----	---	----	4	Jafarpour *et al.*[5,6] (DRS)
	36, 1×10^{-12}	34, 9×10^{-13}	γ and β merge for water > 2 %	85; 5×10^{-20}	84; 3.3×10^{-20}	[E_a=60 kJ/mol for 6% water]	2	Montès *et al.*[13] (low freq. DMA)
	Anti-plasticizing effect: increase of E_a and shift to higher T, *Intensity increases*			Plasticizing effect: decrease of E_a and shift to lower T; I*ntensity increases*			4	Jafarpour *et al* (TSDC)[5,6]
Starch	γ_1: 42, 1.6×10^{-14} γ_2: 25, 2.5×10^{-11}	γ_1: 40, 5×10^{-15} γ_2: 28, 2.5×10^{-12}	γ_1: I*ntensity decreases* γ_2: *Insensitive*	76, 6.3×10^{-17}	53, 2×10^{-17}	Plasticizing effect: Shift to lower T and *Intensity increases*	15.5	Laredo *et al*[51] (TSDC)
Ethyl cellulose	Non-cooperative process; Insensitive to aging			Non-cooperative process; Very sensitive to physical aging			---	Diogo and Moura Ramos[17] (TSDC)
Cellulose acetate (DS=2.45)	46.8, 2.6×10^{-15}	---------	-----	γ-$C_{2,3}$: 50.1, 3×10^{-16} γ-C_6: 44.8, 2.3×10^{-15}	----	Side-groups relaxations of the C_n substituents	--	Einfeldt *et al.*[10] (DRS)
Cellulose actetate (DS=2.45)	**173 K ≤ T ≤ 298 K**			**353 K ≤ T ≤ 443 K**				**this work**
	γ_{dry} [d]	**Wet**		*Weak process appears in the high frequency flank of the α-relaxation compatible with θ_{JG}*			2.73	
	60, 5×10^{-17}	**I (faster)** 44, 3×10^{-16} *Shift to higher f; Intensity increases* **II (slower)** 64, 3×10^{-16} *Small shift to lower f, with water uptake*						

[a] Cellulose acetate studied in this work is also included. [b] The authors called this faster process β-relaxation. [c] As concluded from Figure 2 of ref 6. [d] Processes I and II observed in the wet state merge into a single broad one in the dried state, γ_{dry}; a third low intensity relaxation is visible in its high frequency flank.

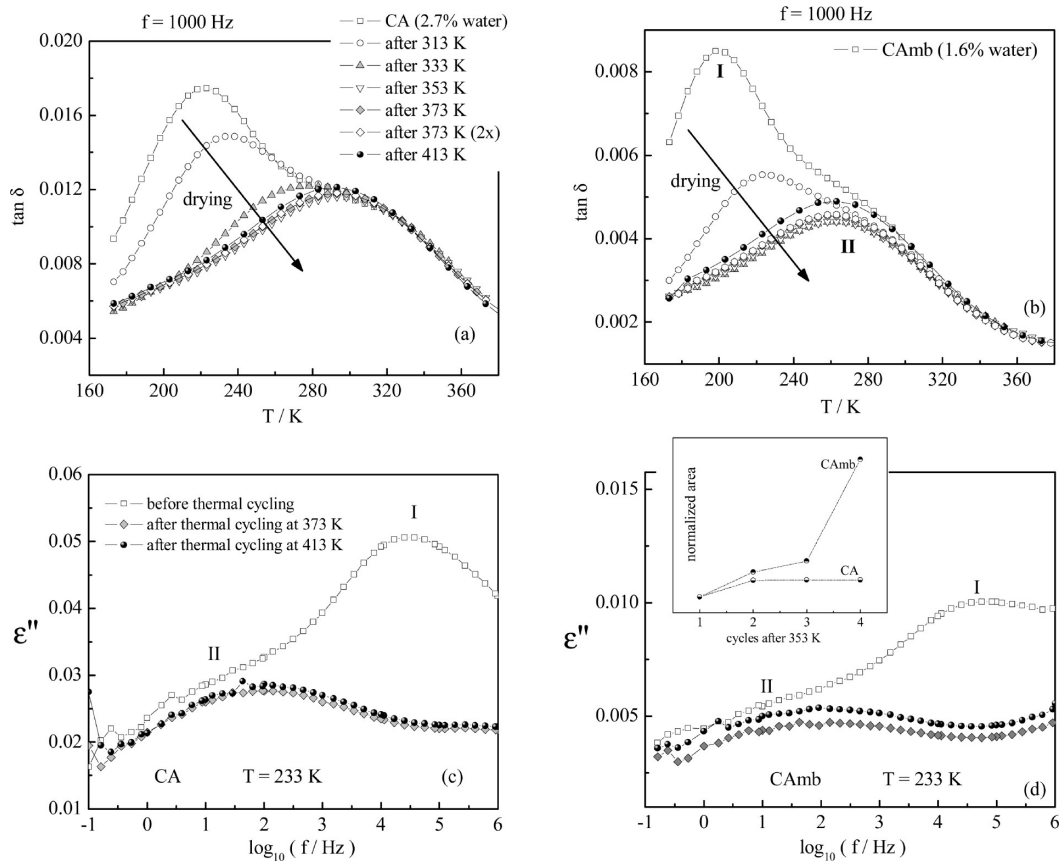

Figure 9. Effect of dehydration on the dielectric response: temperature dependent behavior of tan δ at 1 kHz for (a) CA and (b) CAmb; frequency dependent dielectric loss for (c) CA and (d) CAmb (the symbols in part a apply for all figures). In the inset of part d is plotted the area under the isochronal tan δ (1 kHz) curves normalized for the area under the curve obtained after 353 K, the one from which no more changes in the peak's location occurred for all systems.

present in the membrane sample (<2%). In the above-mentioned studies for cellulose[5,6,13] and starch,[51] the influence of such low water contents is not so obvious in the detected spectra. For different types of cellulose, Einfeldt et al.[20] report that for water contents less than 2−3% no significant differences arise for the relaxation observed at the lowest temperatures (designated β by the authors). The influence of hydration on the activation parameters of this relaxation process is observed only for contents higher than 4%, being highly dependent from the specific morphological order of the cellulose substrate. Due to the great ability of the hydroxyl groups to establish H-bonds, strong intermolecular interactions are present in cellulose. Contrarily, the cellulose acetate samples here studied, with a substitution degree of 2.45, have a completely different material architecture, as discussed before on analyzing the FTIR spectra, with no intermolecular H-bonds. Therefore, more polar groups, either acetyl or hydroxyl, are available for water uptake, resulting in a greater effect of low water contents in cellulose acetate relative to cellulose.

The main observation in Figure 9 is the strong depletion of process I with the increase of the final temperature reached in the preceding run. Instead of two processes as detected in measurements carried out below 298 K, in the dehydrated state, a broad and asymmetric process remains with identical features for both CA and CAmb ($\alpha_{HN} = 0.29 \pm 0.08$ and $\beta_{HN} = 0.41 \pm 0.05$) located roughly at an intermediate temperature/frequency comparing to processes I and II. A very similar behavior was found for another biopolymer, poly(L-lactic acid), PLLA, by some of us.[58]

The progress of the dielectric loss in both CA and CAmb with dehydration can be analyzed in reverse order, starting from the dry state: with a moderate water uptake, the broad process observed in the dehydrated sample becomes more resolved, since water plasticizes process I, shifting its location to lower temperatures (higher frequencies in the isotherms), revealing the underlying process II; the latter undergoes a slight antiplasticizing effect slightly shifting to higher temperatures. Both processes I and II will collapse into a single process at very high temperatures, as deduced from the same value of τ_∞. Therefore, the process after dehydration, that is complex in nature, will have the contribution of the two relaxations observed in the systems with moderate water contents, process I being more critically influenced by the water uptake.

Figure 9c compares at 233 K the dielectric response of CA with that after being submitted to thermal cycling reaching 373 and 413 K. Figure 9d shows the correspondent data for CAmb. The observed behavior seems to corroborate the previous data interpretation. In the moderately hydrated state, the two processes are visible, while, in the dry state, process I is highly depleted and shifted to lower frequencies overlapping with process II; this causes the appearance of a single broad relaxation, designated hereafter as the γ_{dry}-process. The multimodal nature of secondary processes was also observed in moderately hydrated and dry CA,[10,16] starch,[7,51] ethyl cellulose,[17] hydroxypropyl cellulose and dextran,[59] and other biopolymers.[60]

Figure 10 shows the 3D plots for CAmb in a temperature range from 173 to 298 K (a) before and (b) after dehydration achieved by thermal cycling. It nicely illustrates the detection of two relaxations for the sample with moderate water content and the presence of a broad process (γ_{dry}) after thermal treatment.

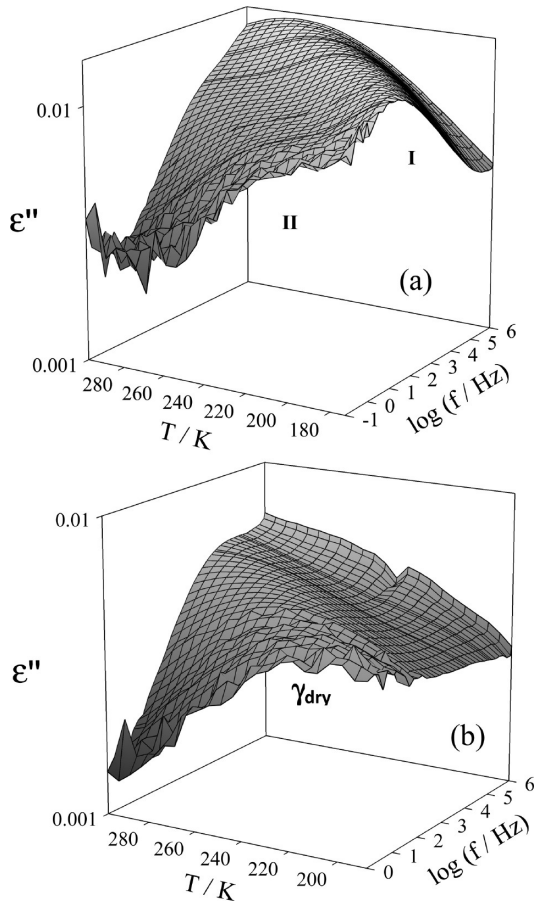

Figure 10. 3D plots of the dielectric loss for the CAmb: (a) before thermal cycling evidencing the two relaxation processes I and II; (b) after thermal cycling up to 413 K where a broad process, γ_{dry}, persists more or less in between processes I and II.

The activation plot for the main process that remains after moisture loss was included in Figure 8a, lying in between the two temperature dependencies found for the hydrated specimens with an activation energy of 60 ± 1 kJ·mol^{-1} for both CA and CAmb (data obtained after second run with $T_f = 373$ K). A summary of the different activation parameters is presented in Table 3.

The overlap of both processes I and II in the dried state is an indication that the respective molecular origins are strongly correlated, in line with the same value of relaxation times at infinite temperature (pre-exponential factor τ_∞) found in the hydrated state. The prefactor of the γ_{dry}-relaxation (5×10^{-17}s) also points in the same direction, being characteristic of an energy distributed process. The detection of the individual contributions in such a process could be achieved by a low frequency technique such as TSDC enabling the resolution of otherwise overlapping processes.

It is worth mentioning that, in dehydrated samples, the presence of an additional process is felt in the high frequency side of the isotherms, perceptible in the right-hand side of Figure 9c and d for samples submitted to thermal treatment. A detailed characterization of this process will not be provided here. Nevertheless, it probably already exists in hydrated samples but is masked by process I.

With respect to the assignment of the individual components I and II, the dehydration experiments and the comparison between CA and CAmb can help to clarify their respective molecular origins.

As seen in the hydrated samples, process I in CA is located at higher frequencies (at the same T) relative to membrane, meaning that the mobility is enhanced in the former. The looser structure of the polymer powder makes it more accessible to polar groups within the monomeric unit to interact with water, thus being able to allocate more water molecules and undergoing a greater plasticizing effect (based on the shift of the relaxation peak). The observed process I must be related with a join effect of the cyclic unit motion and the polar groups that reorientate coupled to it. The plasticization observed for process I upon hydration could be explained by a weakening effect of the intramolecular hydrogen bonds (HBs) that additionally contribute to the rigidity of the main chain structure. In fact, the incoming water molecules, while interacting via HBs with the polar groups directly attached to the anhydroglucose rings, would weaken the pre-existing HBs, thus rendering more mobile the underlying mechanism. The previous FTIR analysis showed that the same weight contribution of the intramolecular components to the global spectrum was found for both CA and CAmb. Therefore, it is not the extent of intramolecular HBs that causes the higher rate of process I in CA; instead, it should be a consequence of the greater number of water molecules that CA can hold and their closeness to the anhydroglucose rings, causing a greater weakening effect over the intra HBs. This hypothetic effect is illustrated in Scheme 4 where the possible molecular conformations of cellulose acetate according the degree of substitution (remember that DS = 2.45 means only 1 OH group per two glucosidic rings) are depicted. The existent intramolecular hydrogen bonds (HB) involving the two anhydroglucose rings (depicted according to the FTIR analysis and identified by one asterisk) become weakened in the wet state due to the interaction with a water molecule that can also establish a HB with the OH(2,3′) groups. It should be pointed out that process I must involve a very limited length scale, as is suggested by its location, far below the glass transition, and the τ_∞ value (3×10^{-16} s) which is relatively close to the Debye value, meaning that is affected by a low entropic contribution.

A different interpretation for the origin of process I as proposed by others[61] is that it is an additional process associated with either reorientation of bound water[62] or glass transition of tightly bounded water.[19,16]

Concerning process II, its evolution upon dehydration rules out the hypothesis of being attributed to a Johari−Goldstein process. In fact, with dehydration, the α-relaxation associated with the dynamic glass transition should be shifted to higher temperatures and, concomitantly, the β_{JG}-process. As previously mentioned, according to the reports by Montès et al.,[13] Jafarpour

TABLE 3: Summary of the Estimated Arrhenius Parameters: Activation Energy, E_a, and Pre-Exponential Factor, τ_∞

	E_a (kJ·mol^{-1}); τ_∞ (s)	
samples (% w/w water)	process I	process II
CA (2.73%)	44.3 ± 0.4; $(3 \pm 1) \times 0^{-16}$	64.3 ± 0.8; $(3 \pm 1) \times 10^{-16}$
CAmb (1.60%)	45.3 ± 0.6; $(3 \pm 1) \times 10^{-16}$	
after dehydration	remaining process (γ_{dry}): 60 ± 1; $(5 \pm 3) \times 10^{-17}$	

SCHEME 4: The Three Possible Molecular Conformations of Cellulose Acetate with DS = 2.45[a]

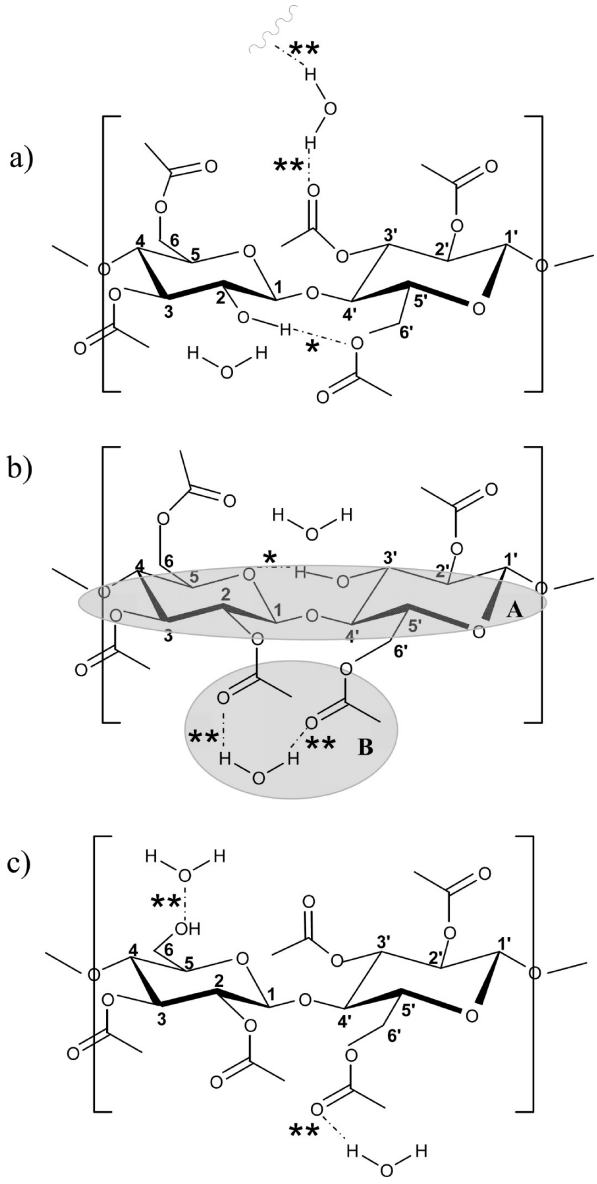

[a] The intramolecular HB, involving the two anhydroglucose rings connected via a glycosidic linkage, are identified by one asterisk in (a) O2−H2···O6′ (corresponding to the intra-chain H-bond ν_1 FTIR band; see the Infrared Spectroscopy section) and (b) O3′−H3′···O5 (corresponding to the intra-chain H-bond ν_2 FTIR band); in part c, the intramolecular bond is absent, since it is not detected by FTIR. In the wet state, these intramolecular HBs become weakened. Examples of the possible HBs between the carbonyl moiety of the acetyl side groups and water are identified with two asterisks. Gray areas A and B illustrate, respectively, the molecular regions where the mechanisms underlying the dielectric processes I and II can predominantly take place. In the dried state, both processes relax in a coupled motion.

et al.,[5,6] and Laredo et al.,[51] this process always becomes faster upon hydration. This is in opposition to the behavior undergone by process II in CA. In order to find the process precursor of the α-relaxation, additional measurements were performed in the dried CA sample by collecting isotherms in the high temperature region up to 473 K. Figure 11 presents the loss curves from 353 to 443 K, in steps of 15 K. The β_{JG}-relaxation is visible, emerging in an intermediate location between the γ_{dry}-process and the incoming α-relaxation in its low frequency side (a detailed analysis will be provided elsewhere). Therefore,

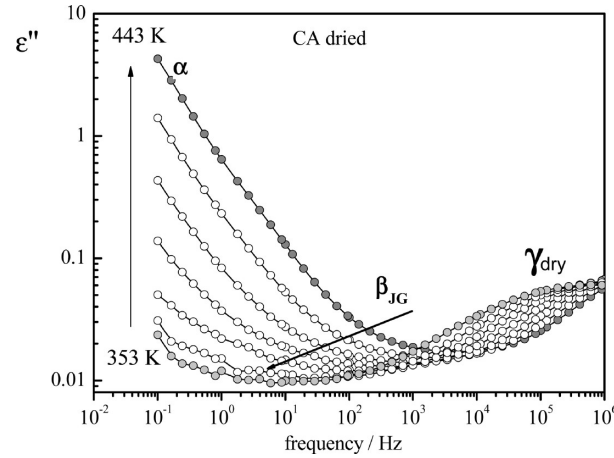

Figure 11. Dielectric loss for dried CA, from 353 to 443 K in steps of 15 K. In the high frequency side of the spectra, the faster relaxation, γ_{dry}, is visible. A weak relaxation is observed between the latter and the high frequency flank of the α-relaxation, identified with the β_{JG}-process.

process II observed in moderately hydrated CA has a different origin. Since it does not present significant differences for the distinct samples, either CA or CAmb, its origin can be due to local motions that may be insensitive to the matrix morphology either as membrane or powder. It may be probably due to the side-group rotations but strongly correlated with the mobility of the cyclic unit itself. Upon hydration, the bulky acetyl groups, which are hydrogen bonding acceptors, can establish weak H-bonds with water molecules as the ones illustrated in Scheme 4, identified by two asterisks. Water can act as a mediator between acetyl groups belonging to either the same cyclic unit or adjacent units, building a network with restricted mobility causing a weak antiplasticizing effect in relaxation process II (shift to lower frequencies).

It is worthwhile to mention that the evolution of dehydration with thermal treatment occurs with different rates while comparing the CA and CAmb. At the run with $T_f = 373$ K, the two processes already converge on a broad process. However, recalling Figure 9a and b, the depletion of process I occurs slower in CA relative to the membrane. This could just originate from the higher water content in CA; however, having in mind that the main differences in the evolution between membrane and powder arise above 333 K, and the time-consuming data acquisition procedure (∼6 min at each scanned temperature), this probably overcomes the difference of 1.4% of the water content of CA relative to CAmb. A different reason for the faster progress with increasing temperature observed for the membrane is that the water molecules probed by DRS which are affecting process I might be less strongly bounded in the membrane in comparison with the powder. This observation is in agreement with DSC thermograms where the minimum of the endotherm due to water removal was located at a lower temperature in CAmb relative to CA (remember Figure 3a). The more disordered structure of CA makes more internal sites accessible to water. Previous NMR analysis by Keely et al.[19] showed that plasticized CA with fillers that promote disorder allow water to associate further to oxygen atoms in the main chain, while in unplasticized samples water associates mainly to the side groups. This effect can be taken as a further indication that some main-chain motion (anhydroglucose ring connected via a glycosidic linkage) is involved in the relaxation mechanism in the origin of process I.

Furthermore, it is interesting to analyze the changes in the magnitude of the broad process that remains after dehydration

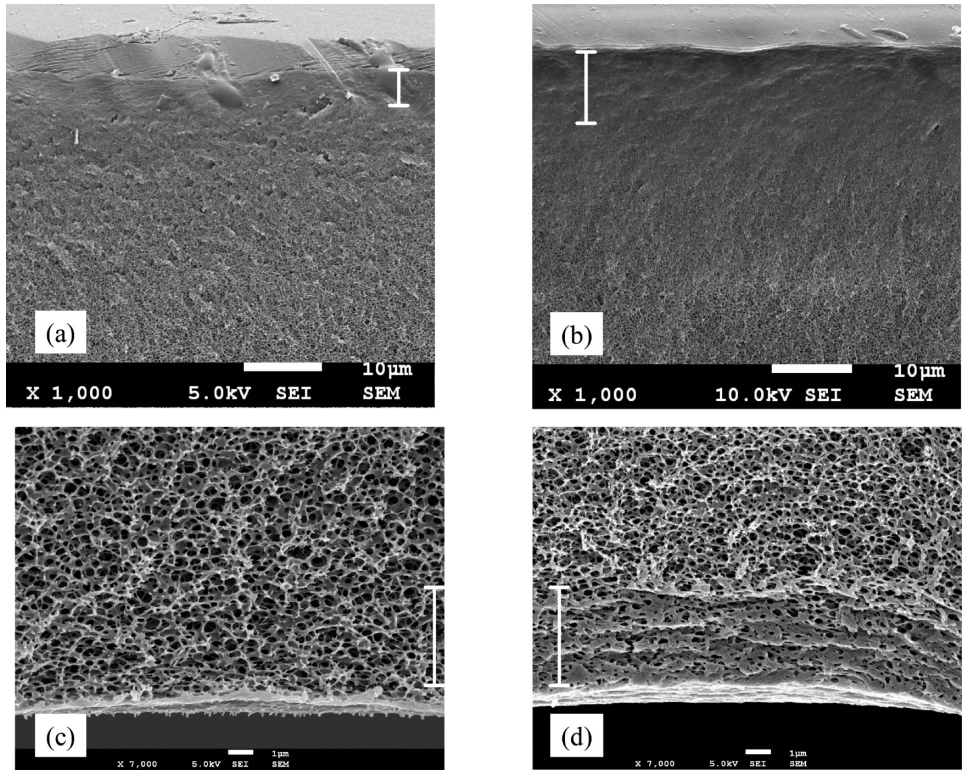

Figure 12. SEM micrographs of the asymmetric CAmb: (a, c) as prepared; (b, d) after thermal treatment up to 413 K; (a, b) top cross section of membrane; (c, d) bottom cross section of membrane. The vertical bars indicated the regions where modifications are more visible.

upon further heating: in CA, the dielectric response keeps almost invariant when the sample is heated up to 413 K; however, in the membrane, there is a continuous increase of intensity, that is even more enhanced after heating up to 413 K. The inset of Figure 9d presents the variation of the area under the isochronal curves, normalized by the area of the curve taken after 353 K (temperature from which no more changes in location occurred for any system); the number of scanned temperature cycles in this region is represented in the *x* axis, cycle 1 corresponding to data obtained after 353 K. While the plot for CA reaches a plateau, an enhancement of the dielectric response in the membrane is observed clearly differentiating it from the CA behavior.

The change in magnitude of the process detected in dry cellulose is reported for different types of cellulose after annealing at 453 K being attributed to the phenomenon of "hornification" which is a morphological effect concomitant to the driving out of residual water (see ref 20 and references therein). In the dried membrane, this effect could be accompanied by a partial destruction of the membrane structure, due to the final removal of water molecules that assured the inner porous architecture. To elucidate this, SEM analysis was carried out for the membrane after being submitted to thermal treatment up to 413 K. Figure 12 shows a scale-up of micrographs taken for CAmb before (a and c) and after (b and d) the thermal treatment. It evidences the changes in the top region that becomes denser and thicker (thickness of this denser region approximately indicated by the size of the bars in parts a and b) and in the bottom part of the membrane, where some collapse of the porous network occurred.

This overall densification of the CAmb structure led to the dielectric loss rising which evolves continuously and is higher than the increase observed for the CA, the latter only occurring after surpassing 413 K. This could be taken as a particular feature of materials structured as membranes where the morphological network modifications occur progressively.

Conclusions

A detailed structural and dynamical characterization of cellulose acetate polysaccharide is provided comparing CA (DS = 2.45) in the powder state with the same CA polymer produced as an asymmetric membrane, assuring that the observed differences are a consequence of the polymeric arrangement; in this context, to our best knowledge, no similar studies can be found in the literature.

In spite of a careful drying process to which membrane was submitted to, a moderate water content was found (1.60% w/w), since once synthesized the membrane readily recaptures water molecules due to its high hydrophilicity. Higher water amount was determined for the CA powder (2.73% w/w). By DSC, both glass transition and melting were observed. The onset of their glass transitions occurs at similar temperatures, 467 K, and equivalent extents of the crystalline phase were determined (14%).

The slight inferior thermal stability (TGA) and broader both melting endotherm (DSC) and FTIR spectrum indicate a less structured chain packing for CA. Therefore, the cellulose acetate polymeric main chains are arranged in a more ordered packing in the CA membrane.

Two subglass relaxation processes were detected by DRS, which emerge at low temperatures (from below 173 K), being able to be observed up to room temperature. It was found that water affects the two relaxation processes differently. While the process that first enters in the frequency window (process I) is highly influenced by water, undergoing a plasticizing effect shifting to higher frequencies (lower *T*), the second process (process II) seems to be less affected, nevertheless in an opposite way: it deviates to lower frequencies (higher *T*), therefore

undergoing an antiplasticizing effect. Process I is more mobile for CA than CAmb, as showed by its shift to higher frequencies at the same *T*, or to lower temperatures at the same *f*. Since the amorphous/crystallinity extent in CA and CAmb are equivalent, the observed differences were rationalized in terms of distinct polymeric arrangements and ability for water takeover. The less ordered packing in CA powder offers more internal sites to be accessible for water uptake, not only by the side groups but also by the polar groups within the anhydroglucose rings playing a more effective plasticizing phenomenon, resulting in an overall enhanced mobility for CA than for CAmb. The results reported here suggest that process I must be related to a join effect of the cyclic unit motion and the polar groups that reorientate coupled to it. Nevertheless, it should involve a very limited length scale, as is suggested by its location, far below the glass transition, and the value found for the pre-exponential factor affected by a low entropic contribution.

Upon hydration, the pre-existing intramolecular bonds become weakened due to establishment of HBs between the oxygen atoms directly attached to the glucosidic rings and the incoming water molecules, enhancing the mobility of the underlying mechanism.

Process II seems to be associated with side-group rotations but strongly correlated with the cyclic unit motion, being more insensitive to both matrix morphology and water content; upon hydration, the water molecules associate via H-bonds with the acetyl groups hindering its mobility.

Both processes seem to be highly correlated collapsing into a broad one, designated γ_{dry}, in the full dried state as monitored by DRS. The respective $(\tau_\infty)\gamma_{dry}$ value is compatible with an energy distributed process coherent with the simultaneous contribution of processes I and II. The detection of the individual components could be achieved by a low frequency technique such as TSDC which enables the resolution of otherwise overlapping processes.

At temperatures above 353 K, a distinct process emerges, with features compatible with the β_{JG}-relaxation precursor of the dynamic glass transition, as found in several saccharides.

Additionally, when membrane is submitted to high temperatures, a partial collapse of their inner porous architecture occurs, resulting in a densification of the structure as confirmed by SEM (taken after 413 K); DRS proved to also be sensitive to this effect that reflects in an accentuated increase in the dielectric response upon heating above 353 K, which does not occur in the CA powder (in the studied temperature range). In spite of the lack of a definitive attribution of the relaxation detected processes, the present work represents an additional contribution, clearly illustrating the dramatic effect of water in the secondary process of moderately hydrated cellulose acetate specimens and evidencing the multimodal nature of the process detected in the dried state.

From the comparison of data in the literature, it is important to point out that the β-process taken as the precursor of the α-relaxation (β_{JG}), to which data provided by different authors are very coherent, should be distinguished from the slower process found in substituted cellulosic materials that is influenced by several factors such as the bulkiness of side groups and degree of substitution. The apparent contradiction in results found for the faster subglass relaxation, mainly how it behaves under hydration, can be related to the amount of water (moderated hydrated samples behave differently from highly wetted materials) and to morphologic differences. From the results reported here, we conclude that small amounts of water can act as a probe of the different sites where water can be absorbed/bounded in such morphological different materials.

Therefore, the demand for a universal description of the behavior in complex systems is not a trivial task, since multiple factors concur to the observed behavior, among which water amount, substitution degree, and even crystallinity degree can play a relevant role.

Acknowledgment. The authors thank Professor Luis Paulo N. Rebelo (ITQB/UNL) for the equipment facilities for thermal analysis. Financial support to Fundação para a Ciência e Tecnologia (FCT, Portugal) through the project PTDC/CTM/64288/2006 is acknowledged. A.R.B. acknowledges FCT for a Ph.D. grant (SFRH/BD/23829/2005).

References and Notes

(1) Guo, Y.; Wu, P. *Carbohydr. Polym.* **2008**, *74*, 509.
(2) Aoki, D.; Teramoto, Y.; Nishio, Y. *Biomacromolecules* **2007**, *8*, 3749.
(3) Radloff, D.; Boeffel, C.; Spiess, H. W. *Macromolecules* **1996**, *29*, 1528.
(4) Meiβner, D.; Einfeldt, L.; Einfeldt, J. *J. Polym. Sci., Part B: Polym. Phys.* **2001**, *39*, 2491.
(5) Jafarpour, G.; Dantras, E.; Boudet, A.; Lacabanne, C. *J. Non-Cryst. Solids* **2007**, *353*, 4108.
(6) Jafarpour, G.; Roig, F.; Dantras, E.; Boudet, A.; Lacabanne, C. *J. Non-Cryst. Solids* **2009**, *355*, 1669.
(7) Butler, M. F.; Cameron, R. E. *Polymer* **2000**, *41*, 2249.
(8) Einfeldt, J.; Meiβner, D.; Kwasniewski, A.; Einfeldt, L. *Polymer* **2001**, *42*, 7049.
(9) Einfeldt, J.; Meiβner, D.; Kwasniewski, A. *J. Non-Cryst. Solids* **2003**, *320*, 40.
(10) Einfeldt, J.; Meiβner, D.; Kwasniewski, A. *Prog. Polym. Sci.* **2001**, *26*, 1419.
(11) Kaminski, K.; Kaminska, E.; Wlodarczyk, P.; Pawlus, S.; Kimla, D.; Kasprzycka, A.; Paluch, M.; Ziolo, J.; Szeja, W.; Ngai, K. L. *J. Phys. Chem. B* **2008**, *112*, 12816.
(12) Kaminski, K.; Kaminska, E.; Ngai, K. L.; Paluch, M.; Wlodarczyk, P.; Kasprzycka, A.; Szeja, W. *J. Phys. Chem. B* **2009**, *113*, 10088.
(13) Montès, H.; Mazeau, K.; Cavaillé, J. Y. *Macromolecules* **1997**, *30*, 6977.
(14) Nishinari, K.; Shibuya, N.; Kainuma, K. *Makromol. Chem.* **1985**, *186*, 433.
(15) Bidault, O.; Assifaoui, A.; Champion, D.; Le Meste, M. *J. Non-Cryst. Solids* **2005**, *351*, 1167.
(16) McBrierty, V. J.; Keely, C. M.; Coyle, F. M.; Xu, H.; Vij, J. K. *Faraday Discuss.* **1996**, *103*, 255.
(17) Diogo, H. P.; Moura-Ramos, J. J. *J. Polym. Sci., Part B: Polym. Phys.* **2009**, *47*, 820.
(18) Hinterstoisser, B.; Åkerholm, M.; Salmén, L. *Biomacromolecules* **2003**, *4*, 1232.
(19) Keely, C. M.; Zhang, X.; McBrierty, V. J. *J. Mol. Struct.* **1995**, *355*, 33.
(20) Einfeldt, J.; Kwasniewski, A. *Cellulose* **2002**, *9*, 225.
(21) Puleo, A. C.; Paul, D. R.; Kelley, S. S. *J. Membr. Sci.* **1989**, *47*, 301.
(22) Loeb, S.; Sourirajan, S. *Sea Water Demineralization by Means of an Osmotic Membrane. Saline Water Conversion—II*; Advances in Chemistry, vol. 38; American Chemical Society: Washington, DC, 1963; Chapter 9, pp 117−132.
(23) Dias, C. R.; Rosa, M. J.; de Pinho, M. N. *J. Membr. Sci.* **1998**, *138*, 259.
(24) Wydeven, T.; Leban, M. *J. Appl. Polym. Sci.* **1973**, *17*, 2277.
(25) Murphy, D.; de Pinho, M. N. *J. Membr. Sci.* **1995**, *106*, 245.
(26) Kesting, R. *Synthetic Polymeric Membrane*; McGraw-Hill: New York, 1971.
(27) Matsuura, T.; Sourirajan, S. *Fundamentals of Reverse Osmosis*; National Research Council of Canada: Ottawa, Canada, 1985.
(28) de Pinho, M. N. *Desalination* **1988**, *68*, 211.
(29) Rosa, M. J.; de Pinho, M. N. *J. Membr. Sci.* **1994**, *89*, 235.
(30) Lui, A.; Talbot, F. D. F.; Fouda, A.; Matsuura, T.; Sourirajan, S. *J. Appl. Polym. Sci.* **1988**, *36*, 1809.
(31) Kulkarni, S.; Krause, S.; Wignall, G. D.; Hammouda, B. *Macromolecules* **1994**, *27*, 6777.
(32) Havriliak, S.; Negami, S. *Polymer* **1967**, *8*, 161. Havriliak, S.; Negami, S. *J. Polym. Sci., Part C: Polym. Symp.* **1966**, *14*, 99.

(33) Schönhals, A.; Kremer, F. Analysis of Dielectric Spectra. In *Broadband Dielectric Spectroscopy*; Schönhals, A., Kremer, F., Eds.; Springer-Verlag: Berlin, 2003; Chapter 3.

(34) (a) Boersema, A.; van Turnhout, J.; Wübbenhorst, M. *Macromolecules* **1998**, *31*, 7453. (b) Schröter, K.; Unger, R.; Reissig, S.; Garwe, F.; Kahle, S.; Beiner, M.; Donth, E. *Macromolecules* **1998**, *31*, 8966.

(35) Kamide, K. *Cellulose and cellulose derivatives molecular characterization and its applications*; Elsevier: The Netherlands, 2005.

(36) Scandola, M.; Ceccorulli, G. *Polymer* **1985**, *26*, 1953.

(37) Barud, H. S.; de Araújo Júnior, A. M.; Santos, D. B.; de Assunção, R. M. N.; Meireles, C. S.; Cerqueira, D. A.; Rodrigues Filho, G.; Ribeiro, C. A.; Messaddeq, Y.; Ribeiro, S. J. L. *Thermochim. Acta* **2008**, *471*, 61.

(38) Cerqueira, D. A.; Rodrigues Filho, G.; Assunção, R. M. N. *Polym. Bull.* **2006**, *56*, 475.

(39) Filho, G. R.; Bueno, W. A. *J. Membr. Sci.* **1992**, *74*, 19.

(40) Toprak, C.; Agar, J. N.; Falk, M. *J. Chem. Soc., Faraday Trans. 1* **1979**, *75*, 803.

(41) Ilharco, L. M.; Brito de Barros, B. *Langmuir* **2000**, *16*, 9331.

(42) Statton, W. O. *J. Appl. Polym. Sci.* **1963**, *7*, 803.

(43) Kataoka, Y.; Kondo, T. *Macromolecules* **1998**, *31*, 760.

(44) Dawy, M.; Nada, A.-A. M. A. *Polym.-Plast. Technol. Eng.* **2003**, *42*, 643.

(45) Åkerholm, M.; Hinterstoisser, B.; Salmén, L. *Carbohydr. Res.* **2004**, *339*, 569.

(46) Starkweather, H. W., Jr. *Polymer* **1991**, *32*, 2443.

(47) Kaminski, K.; Kaminska, E.; Hensel-Bielowka, S.; Pawlus, S.; Paluch, M.; Ziolo, J. *J. Chem. Phys.* **2008**, *129*, 084501.

(48) van Dusschoten, D.; Tracht, U.; Heuer, A.; Spiess, H. W. *J. Phys. Chem. A* **1999**, *103*, 8359.

(49) Kaminski, K.; Kaminska, E.; Grzybowska, K.; Wlodarczyk, P.; Pawlus, S.; Paluch, M.; Ziolo, J.; Rozska, S. J.; Pilch, J.; Kasprzycka, A.; Szeja, W. Transformation of the Strongly Hydrogen Bonded System into van der Waals one Reflected. In *Molecular Dynamics Metastable systems under pressure*; Rzoska, S., Drozd-Rzoska, A., Mazur, V., Eds.; W. NATO Science for Peace and Security Series A: Chemistry and Biology; Springer: The Netherlands, 2010; p 359.

(50) Einfeldt, J.; Meiβner, D.; Kwasniewski, A. *Cellulose* **2004**, *11*, 137.

(51) Laredo, E.; Newman, D.; Bello, A.; Müller, A. J. *Eur. Polym. J.* **2009**, *45*, 1506.

(52) Ngai, K. L. *J. Phys.: Condens. Matter* **2003**, *15*, S1107.

(53) Eyring, H. *J. Chem. Phys.* **1936**, *4*, 283.

(54) According to Figure 2 of ref 6.

(55) Noel, T. R.; Parker, R.; Ring, S. G. *Carbohydr. Res.* **2000**, *329*, 839.

(56) Kaminski, K.; Kaminska, E.; Paluch, M.; Ziolo, J.; Ngai, K. L. *J. Phys. Chem. B* **2006**, *110*, 25045.

(57) Diogo, H. P.; Moura-Ramos, J. J. *Carbohydr. Res.* **2008**, *343*, 2797.

(58) Braś, A. R.; Viciosa, M. T.; Dionisio, M.; Mano, J. F. *J. Therm. Anal. Calorim.* **2007**, *88*, 425.

(59) Shinouda, H. G.; Abdel Moteleb, M. M. *J. Appl. Polym. Sci.* **2005**, *98*, 571.

(60) Braś, A. R.; Malik, P.; Dionisio, M.; Mano, J. F. *Macromolecules* **2008**, *41*, 6419.

(61) Cerveny, S.; Schwartz, G. A.; Bergman, R.; Swenson, J. *Phys. Rev. Lett.* **2004**, *93*, 245702.

(62) Schartel, B.; Wendling, J.; Wendorff, J. H. *Macromolecules* **1996**, *29*, 1521.

JP101665H